HHS Public Access

Author manuscript

IEEE Trans Ultrason Ferroelectr Freq Control. Author manuscript; available in PMC 2018 November 01.

Published in final edited form as:

IEEE Trans Ultrason Ferroelectr Freq Control. 2017 November ; 64(11): 1684–1697. doi:10.1109/TUFFC.2017.2748050.

Catheter Hydrophone Aberration Correction for Transcranial Histotripsy Treatment of Intracerebral Hemorrhage (ICH): Proof-of-Concept

Tyler Gerhardson,
Department of Biomedical Engineering, University of Michigan, Ann Arbor, MI, 48109, USA

Jonathan R. Sukovich,
Department of Biomedical Engineering, University of Michigan, Ann Arbor, MI, 48109, USA

Aditya S. Pandey,
Department of Neurosurgery, University of Michigan, Ann Arbor, MI 48109 USA

Timothy L. Hall,
Department of Biomedical Engineering, University of Michigan, Ann Arbor, MI, 48109, USA

Charles A. Cain [Fellow, IEEE], and
Department of Biomedical Engineering, University of Michigan, Ann Arbor, MI, 48109, USA

Zhen Xu [Member IEEE]
Department of Biomedical Engineering, University of Michigan, Ann Arbor, MI 48109 USA

Abstract

Histotripsy is a minimally invasive ultrasound therapy that has shown rapid liquefaction of blood clots through human skullcaps in an in-vitro intracerebral hemorrhage (ICH) model. However, the efficiency of these treatments can be compromised if the skull induced aberrations are uncorrected. We have developed a catheter hydrophone which can perform aberration correction and drain the liquefied clot following histotripsy treatment. Histotripsy pulses were delivered through an excised human skullcap using a 256-element, 500 kHz hemisphere array transducer with a 15 cm focal distance. A custom hydrophone was fabricated using a 0.5 × 0.5 × 0.3 mm PZT-5h crystal interfaced to a coaxial cable and integrated into a drainage catheter. An aberration correction algorithm was developed to correct the aberrations introduced between histotripsy pulses from each array element. Increases in focal pressure of up to 60% were achieved at the geometric focus and 27 – 62% across a range of electronic steering locations. The sagittal and axial −6 dB beam widths decreased from 4.6 to 2.2 mm in the sagittal direction and 8 to 4.4 mm in the axial direction, compared to 1.5 mm and 3 mm in the absence of aberration. After performing aberration correction, lesions with diameters ranging from 0.24 mm to 1.35 mm were generated using electronic steering over a 10 × 10 mm grid in a tissue mimicking phantom. An average volume of 4.07 ± 0.91 mL was liquefied and drained after using electronic steering to treat a 4.2 mL spherical volume in *in-vitro* bovine clots through the skullcap.

Disclosure notice: Drs. Charles A. Cain, Timothy L. Hall, and Zhen Xu have financial interests and/or other relationship with HistoSonics Inc.

Index Terms

Histotripsy; intracerebral hemorrhage; cavitation; aberration correction; catheter hydrophone

I. Introduction

Hemorrhagic stroke or intracerebral hemorrhage (ICH) accounts for about 15% of all strokes and affects roughly two million people worldwide [1–3]. ICH is caused by the rupture of blood vessels within the brain thus leading to the accumulation of blood products within the brain parenchyma. The initial injury post bleed leads to a mass-occupying lesion and thus mechanical injury of adjacent neurons, axons and supporting cellular matrix. In addition, the presence of the ICH leads to a rise in intracranial pressure (ICP) which in turn leads to a decrease in cerebral perfusion pressure and related ischemia. The secondary injury to the brain occurs over days and weeks and is caused by the cytotoxicity related to metabolism of red blood cell components, specifically hemoglobin. This combination of primary and secondary injuries associated with ICH leads to an approximate 30-day mortality rate of 40% [4–5].

The standard clinical treatments for ICH consist of either medical management to optimize cerebral blood flow (CBF) while decreasing intracranial pressure (ICP) or a craniotomy surgery to remove the ICH [6–9]. Medical management may be sufficient for small ICH but to normalize ICP as well as to prevent secondary injuries, it is essential to remove the clot burden. Craniotomy surgery provides quick access for clot evacuation, but it is highly invasive leading to additional damage as normal cerebral tissue must be traversed, and an evaluation on its effectiveness for a large number of cases remains inconclusive [10–13].

Minimally invasive clot evacuation techniques using thrombolytic drugs and catheters have been gaining clinical support and are currently undergoing clinical trials [14–16]. The most common approach utilizes a ventriculostomy catheter placed within the clot and the administration of thrombolytic drugs, such as recombinant tissue plasminogen activator (rt-PA), allowing liquefaction and drainage of the clot. Although early patient outcomes have shown promise in reducing clot size, the functional outcome of ICH survivors has not improved. While this is a minimally invasive technique, it takes days (3–7) to evacuate the ICH and there are hemorrhagic complications that are related to the administration of thrombolytic drugs. For small blood clots in ischemic stroke, these techniques have been combined with low-amplitude ultrasound pulses with and without contrast agents [17–23]. Although these techniques have an improved treatment rate relative to those used for ICH, such an approach remains limited for treating the large clots characteristic of ICH by the lack of perfusion of the microbubbles and drugs into the interior of the clot. In addition, the drugs used have a high risk of rebleed, adverse localized edema and swelling side effects.

Magnetic resonance guided focused ultrasound (MRgFUS) has recently been developed to assist minimally invasive clot evacuation techniques used to treat ICH however treatment times are long and the process leads to overheating the skull. Animal and human cadaver studies have shown that applying MRgFUS outside the skullcap can liquefy clots without the need for thrombolytic drugs [24–25]. The resulting liquid can then be aspirated out with a

needle. Although MRgFUS has shown the ability to shorten the clot reduction time, the use of pulses greater than 100 μs at a relatively high duty cycle (10%) limit the treatment range within the skull and present an issue of the skull overheating [24, 27–29]. Furthermore, the need for costly MR imaging for the entire MRgFUS treatment is a roadblock for any future widespread clinical adaption.

Histotripsy is a focused ultrasound technology that controls cavitation to liquefy soft tissue such as clots. Histotripsy uses short, high energy pulses to generate cavitation microbubble clouds using the intrinsic nuclei existing in the target tissue [30–33]. High stress and strain is generated in tissue at the focus due to the rapid bubble expansion and collapse that fractionates the tissue into an acellular homogenate [34]. The ability to liquefy clots using histotripsy has been demonstrated in leg vessels both *in-vitro* and *in-vivo* [35–41]. Histotripsy and boiling histotripsy were also reported to treat an *in-vitro* model of large extravascular hematomas in the absence of aberration [42]. Recent work has shown the *in-vitro* feasibility of histotripsy as a transcranial therapy [43–44]. We have also shown the ability to liquefy clots through excised human skullcaps using histotripsy in an *in-vitro* study [45]. Similar to MRgFUS, histotripsy can be used to liquefy clots through the skull. The liquefied volume can then be aspirated via a catheter inserted into the clot through a small bur hole. The purpose of this study was to propose a solution to the problem of skull aberrations in developing histotripsy as a minimally invasive technology for treating ICH.

One significant barrier in developing focused ultrasound technologies for ICH and other transcranial therapies is the ultrasound distortion induced by the skull. Due to sound speed and thickness inhomogeneities inherent to the skull, both MRgFUS and histotripsy suffer from ultrasound defocusing caused by skull-induced acoustic aberration. This causes significant focal amplitude loss and beam widening, resulting in an overall decrease in treatment efficacy and precision [46–47]. MRgFUS is capable of correcting for skull induced acoustic aberrations using MRI guidance and computed tomography (CT) scans obtained prior to treatment. However, this technique requires a sophisticated algorithm, significant treatment planning and extensive MRI time required for MRgFUS treatment leading to a prohibitively high cost. Moreover, these aberration corrections degrade if the skull moves with respect to the transducer. MR acoustic radiation force imaging (MR-ARFI) techniques can outperform CT methods and overcome issues of degraded corrections associated with potential movements of the skull [48]. However, this technique still relies on MRI making it expensive and potentially difficult to adopt.

Many other approaches have been investigated to overcome the skull-induced acoustic aberration for transcranial applications of focused ultrasound with varying degrees of success. Simulation techniques are completely noninvasive and use computed tomography (CT) images of the skull obtained prior to treatment to derive the thickness and acoustic properties of the skull to approximate the aberration through the skull and correct for it [49–53]. These techniques have shown good corrections [54]. However, these techniques require significant treatment planning and time (i.e., 2 hours to execute the simulation) [55]. Furthermore, the difference in position of a patient's head between prior scans and treatment can lead to error. Time reversal techniques involve (1) acquiring a signal transmitted through the skull to or from a single point within the field (2) time reversing the signals and (3) re-

emitting the signals by the elements of the array [56–63]. Variations of acoustic sources and reflectors placed at the focus have been examined *in-vitro* including implanted hydrophones and acoustic stars [64–66]. Hydrophones allow measurement of the waveform timing information with a high degree of accuracy and are a consistent reference for various aberration correction techniques, thus aberration correction using a hydrophone as a receiver remains a near optimal correction technique.

A catheter hydrophone solution for aberration correction in histotripsy treatment of ICH was devised based on two considerations. First, the mainstay minimally invasive approach to ICH treatment already requires inserting a catheter through a small bur hole in the skull to drain the liquefied clot. Second, aberration correction with a hydrophone is considered a near optimal aberration correction technique. A miniature acoustic hydrophone integrated into a drainage catheter provides the ability to conduct the aberration correction necessary for histotripsy treatment while simultaneously providing a means to drain the liquefied clot volume. Since commercial hydrophones are too large to fit within catheters used in minimally invasive brain surgery (I.D. ~ 2 mm), we needed to fabricate our own miniature hydrophone that could fit inside a catheter. The primary goals of this initial study were (1) to fabricate a hydrophone small enough to fit within a catheter and (2) to show the proof-of-concept of using a catheter hydrophone aberration correction technique for transcranial histotripsy ICH treatment.

II. Materials and Methods

A. Experimental Equipment

Transcranial Phased Array Transducer—A 500 kHz 256-element hemispherical transcranial histotripsy array with 15 cm focal distance was used in this study. The array was built in our lab using similar methods as those described in [70]. The individual elements populating the array were comprised of two 1 MHz 20 mm diameter flat, stacked piezo ceramic discs (PZ36, Ferroperm, Kvistgaard, Denmark) that produced a combined center frequency of 500 kHz. The array was placed into a water tank with base dimensions of 60 × 60 cm and height of 40 cm. Degassed water was added to the tank such that the level was approximately 1 cm from the top of the tank. A 256-channel high voltage pulser, capable of delivering short (≤ 2 acoustic cycles) high amplitude ultrasound pulses, was used to drive the elements of the array. The pulser was connected to a field-programmable gated array (FPGA) board (Altera DE1, Terasic Technology, Dover, DE, USA) which was used to independently control each element of the array. The clock speed of the FPGA was100 MHz, giving the driver a temporal precision of 10 ns. Histotripsy pulse sequence parameters were defined through a custom MATLAB (MathWorks, Natick, MA, USA) program and uploaded to the FPGA board.

Catheter Hydrophone Fabrication—A custom, miniature hydrophone integrated with a silicone rubber drainage catheter capable of performing aberration correction and draining liquefied clot was fabricated in our lab. The main challenge in fabricating this hydrophone was keeping the piezoelectric element of the hydrophone small enough to fit within the catheter (2 mm I.D.) while maintaining high enough sensitivity to measure acoustic

waveforms through the skull. Due to its high coupling coefficient and high sensitivity, PZT-5h was used as the piezoelectric element. A 0.5 × 0.5 mm chip of PZT-5h (Steminc-Piezo, Miami, FL) was diced from a larger 0.3 mm thick wafer using a razor blade. The dimensions of the crystal were made as small as possible with respect to the wavelength of the transducer's operating frequency in attempt to establish a point-receiver measurement technique. The PZT chip was interfaced to a coaxial cable by soldering the positive and ground leads of a 1.77 mm O.D. coaxial cable to the respective silver electrodes on the opposing 0.5 × 0.5 mm faces of the PZT-5h crystal (Fig. 1). The crystal and its point of attachment to the cable were coated with epoxy (Loctite E-00NS, Düsseldorf, Germany) such that the epoxy layer was flush with the casing of the coaxial cable and all electrically conductive components were sealed. Any visible bubbles surrounding the crystal-cable interface were removed prior to the epoxy curing. After the epoxy cured, the crystal-cable assembly was inserted fully into the drainage catheter so that the tip of the assembly touched the end of the catheter. The coaxial cable acted as the guide wire to guide the assembly through the catheter. With the exception of those presented in the *Hydrophone Characterization – Time-of-flight Measurements and Directivity* section, all experiments using the catheter hydrophone were performed with the miniature hydrophone inserted into the catheter sheath. In that section, the measurements were done without the sheath because the catheter hydrophone could not be accurately rotated 180° given our current setup, which was necessary for characterizing the directivity of the hydrophone.

B. Hydrophone Characterization

Noise Characterization—To perform aberration correction it was important that the catheter hydrophone had sufficient signal-to-noise ratio (SNR) as to distinguish characteristic features (e.g., peak negative pressure) from the waveform of each individual element. Such features were used as reference points to obtain the corrective delays among the 256 individual element waveforms transmitted through the skull. An average signal-to-noise ratio (SNR) was obtained by averaging the SNR for each of the 256 single element waveforms measured with the catheter hydrophone. SNR calculations were performed by measuring the ultrasound pulse signal from each of 256 individual elements while operating the array at pressure conditions comparable to those used in transcranial treatment. A signal with the array powered off was obtained as the pure noise reference. To understand the attenuation effects of the catheter sheath, the average insertion loss (i.e., pressure decrease with the catheter sheath surrounding the miniature hydrophone relative to the miniature hydrophone without the sheath) from all 256 waveforms was measured.

Time-of-flight Measurements and Directivity—Since intrinsic threshold histotripsy relies on the amplitude of the peak-negative pressure, the efficacy of aberration correction using our catheter hydrophone was dependent on its ability to temporally align the peak-negative pressure from the individual element waveforms. To understand our hydrophone's ability to align these signals, it was important to quantify any variation in the peak-negative pressure time-of-flight as a function of the angle of ultrasound propagation from the array with respect to the catheter hydrophone. Due to the hemispherical shape of the array, the angle of the pulse received by the hydrophone from the elements varied from 0 – 360 degrees. Time-of-flight measurements acquired with the catheter hydrophone (without the

catheter sheath) were compared to those made with a PVDF capsule hydrophone (HGL200, Onda, Sunnyvale, CA, USA), which has minimal variability in the time-of-flight as a function of angle of ultrasound propagation. The catheter sheath was excluded from these measurements because the catheter hydrophone could not be accurately rotated 180° in the catheter sheath with our current setup. Any directivity shown in this measurement was therefore inherent to the custom hydrophone in the absence of the sheath. Each hydrophone was positioned to the geometric origin of the array by performing 3-axis beam scans of the pressure field and moving the hydrophone to the location of the peak-negative pressure. The 256 individual elements of the array were then fired individually, one-at-a-time and the time-of-flight of each pulse from the array to the geometric focus was measured. This experiment was repeated using our catheter hydrophone. To ensure that the catheter hydrophone was "finding" the same focus as the capsule hydrophone during the preliminary scans and that variations in the time-of-flight measurements were not a result of discrepancies in position between the hydrophones within the array, the catheter hydrophone was rotated 180° with respect to the array and measurements were repeated. A set of angular dependent delays was calculated by subtracting the catheter hydrophone measured peak-negative pressure time-of-flight from that of the capsule hydrophone.

C. Sample Preparation

Skullcap Preparation—As the presence of extracranial tissue (i.e., skin and brain) was expected to be a minor source of aberration relative to the skull, experiments were conducted using an excised human skullcap. The skullcap obtained through the University of Michigan Anatomical Donations Program. The skullcap was defleshed and cleaned after extraction and continuously kept in water thereafter. Prior to experiments the skullcap was degassed inside a vacuum chamber for a minimum of a week. A 3D laser scan (Ultra HD 2020i, NextEngine, Santa Monica, California) of the skullcap was used to map the skullcap into 256 discrete thickness values that corresponded to the region of skullcap centered around the ray from each element based on concentric positioning of the skullcap within the array.

Red Blood Cell (RBC) Phantom Preparation—RBC phantoms were used to analyze the size of lesions generated through the skull using histotripsy pulses. RBC phantoms were prepared from an agarose-saline mixture and RBCs following previously established protocols [67]. These phantoms consisted of three layers: a very thin (~500 μm) RBC-agarose gel layer sandwiched between two transparent agarose gel layers (~10 mm thick). The RBC-agarose gel layer provided contrast for indicating cavitation damage. That is, the RBC-agarose gel layer changed from translucent and red to transparent and colorless following the RBC lysis that resulted from cavitation-induced lysis of RBCs.

Blood Clot Preparation—The capability of the catheter hydrophone aberration correction for transcranial histotripsy clot liquefaction was evaluated through *in-vitro* experiments using bovine blood clots. Bovine blood was harvested from a local abaittor and mixed with citrate phosphate dextrose (CPD) (Boston Bioproducts, Ashland, MA, USA) with a CPD-to-blood ratio of 1:9 (v:v) to prevent it from clotting during transport and storage. The blood was stored at 4 °C prior to usage and used within two weeks of harvesting. Clots were prepared by mixing 75 mL of degassed bovine blood and 3 mL of

calcium chloride (#21107, Sigma-Aldrich Co., St. Louis MO, USA) for a final concentration of 20 mM/L. The 78 mL blood/$CaCl_2$ mixture was poured into a latex condom and tied off to form a 50 mm diameter sphere shaped volume. The clots were placed into a water bath kept at 38.6 °C for 6 hours to solidify. Solidified clots were transferred to a refrigerator at 4 °C for 12 hours prior to treatment. Before treatment clots were brought to room temperature (~23 °C).

D. Catheter Hydrophone Measurements and Aberration Correction

Catheter Hydrophone Measurements—The skullcap was positioned concentrically within the array and aligned such that the plane along which it was cut lie 10 mm beyond the plane of the outermost elements of the array. This positioning, with the geometric focus near the center of the skull, corresponds to one which will potentially be used to treat the majority of ICH cases in future *in-vivo* and clinical applications [72–73]. The catheter hydrophone was then positioned to the geometric origin of the array by performing 3-axis beam scans of the pressure field and moving the hydrophone to the location of the peak-negative pressure (Fig. 2). The 256 individual elements of the array were then triggered one-at-a-time to emit histotripsy pulses which were measured with the catheter hydrophone. A total of 50 waveforms were acquired from each of the 256 elements of the array and averaged together to generate a single waveform for each element. The entire acquisition took about 10 minutes. The 256 waveforms were then loaded into the aberration correction algorithm used to perform aberration correction.

Aberration Correction—An aberration correction algorithm was designed to calculate the delays required to align the peak-negative pressure of the 256 waveforms acquired through the skull to geometric origin of the array. The aberration correction algorithm consisted of 4 steps. 1) A first order bandpass filter with a passband between 100 and 850 kHz was used to reduce the noise in the waveforms. 2) The time points of the peak negative values of the pressure were then found for each of the 256 elements of the array. 3) The requisite delays for aberration correction (i.e., how long the firing times of each element must be delayed with respect to one another in order to ensure their concurrent arrival at the focus) were then calculated with respect to the time point at which the peak negative value from an arbitrary reference element was recorded from step 2. This was done by subtracting each of the 256 measured delays from the reference value. 4) To ensure that the calculated delays were within a reasonable time window given the known characteristics of the skullcap (thickness and sound speed) and histotripsy waveforms, a windowing function was used to exclude delays that fell outside of a 4 μs window centered about the mean of the calculated delays. This 4 μs window is currently based on a calculation of the largest expected delay based on the maximum and minimum thickness (11.1 and 2.6 mm, respectively) of the specific skullcap used and an average sound speed (2300 m/s) taken from the literature [77]. As the sound speed is not specific to the skullcap and also various throughout the skullcap, we expect some degree of error in the exclusion of waveforms. Such delays were expected to be calculated from signals with low SNR where variability in noise peaks could alter the true delay calculation. Delays excluded by the windowing function were set equal to that of their nearest neighboring element. Due to restrictions on the minimum (0 μs) and maximum (68 μs) relative delays between the firing times of

individual elements imposed by the FPGA, a fixed offset was then applied to the delay set such that the minimum delay was 0 μs. The final delay set was then uploaded to the FPGA boards and set as a fixed temporal offset to the triggering times of each element.

E. Evaluation of Catheter Hydrophone Aberration Correction

Focal Pressure Measurements—To characterize the alignment of the waveforms at the focus and ultimately the peak-negative pressure recovered due to aberration correction, the transcranial focal pressure was measured under conditions where the array was operated with and without aberration correction. For the transcranial case without aberration correction, the 256 elements of the array were triggered in unison. For the transcranial case with aberration correction, each element was delayed by its respective delay calculated using the aberration correction algorithm and catheter hydrophone measurements. Focal pressure waveforms with aberration correction were obtained using measurements made with both the catheter hydrophone and PVDF capsule hydrophone. To ensure cavitation did not disrupt measurements, pressure measurements were obtained below 20 MPa using a fiber optic hydrophone (FOPH) built in-house [71]. For measurements above the intrinsic threshold, cavitation exists 100% of the time, thus rarefactional pressures beyond 26–30 MPa are unlikely to be generated or measured. Due to this, precise measurements of peak-negative pressures nearing or beyond the intrinsic threshold cannot be made and as such, those peak-negative pressures beyond 20 MPa stated throughout this paper are estimated by linear summation of the measured peak-negative pressure amplitudes of the individual transducer elements. These pressure extrapolations are intended only as indications of the likelihood of cavitation in the focal region and pressure overhead during treatment. For peak-negative pressures below 20 MPa, the focal pressure obtained from the linear summation method matches well with the direct FOPH measurements.

Beam Profiles—To further characterize the extent to which aberration correction realigned the waveforms at the focus, one-dimensional (1D) beam profiles in the absence of aberration and through the skullcap with and without aberration correction were obtained. Beam profiles were measured at low pressure (i.e., < 2 MPa) using a PVDF capsule hydrophone (HGL200, Onda, Sunnyvale, CA, USA). For the case where aberration was absent and transcranial case without aberration correction, the 256 elements of the array were triggered in unison. For the transcranial case with aberration correction, each element was delayed by its respective delay calculated using the aberration correction algorithm and the catheter hydrophone measurements. The hydrophone was positioned to the focus and scanned ± 25 mm from the geometric origin in 0.25 mm steps in the sagittal, coronal and axial directions. For each case, the −6 dB beam width was measured.

Pressure vs. Electronic Focal Steering—To understand the extent to which aberration correction performed at a single position (i.e., the geometric origin) improved the electronic focal steering of the array transcranially, the focal pressure as a function of electronic focal steering position was measured with and without aberration correction across a range of steering locations. For the case without aberration correction, the 256 elements of the array were triggered in unison. For the case with aberration correction, the individual element delays calculated using the catheter hydrophone measurements performed *only* at the

geometric origin of the array were added to the delays for each steered location. The array was steered ± 20 mm from the geometric origin in 1 mm steps in the sagittal, coronal and axial dimension. For each driving condition at each steering position a PVDF capsule hydrophone was positioned to the steering location and used to measure the peak-negative pressure.

Lesion Generation using Electronic Focal Steering—To further evaluate single point aberration correction with the catheter hydrophone, lesions were generated transcranially in an RBC phantom at a range of steering locations. The individual element delays calculated using the catheter hydrophone measurements performed *only* at the geometric origin of the array were again added to the steering delays for each steered location. An RBC phantom was positioned into the skullcap with the RBC-agarose gel layer in plane with the sagittal-coronal plane of the array. Using electronic focal steering, the focus was steered through a 9 × 9 grid of steering positions: ± 10 mm from the geometric origin in 2.5 mm steps in the sagittal and coronal direction. 200 histotripsy pulses were applied to each point at a linearly extrapolated peak-negative pressure of 36 MPa as measured through the skullcap at the geometric origin of the array. Pulses were delivered to each point at a pulse repetition frequency (PRF) of 0.5 Hz. Following lesion generation, the RBC phantoms and corresponding lesions were placed on a light table and imaged. Post-processing of optical images was done using MATLAB in a method similar to that described in previous papers [68–69]. Images were grey-scaled and lesions were circled. The area and diameter of lesions was determined by calibrating the pixel size and counting the number of white pixels.

In-vitro Clot Treatment using Electronic Focal Steering—To show the effects of transcranial histotripsy with catheter hydrophone aberration correction in treating ICH an *in-vitro* bovine clot ICH model was developed and treated using transcranial histotripsy. Following aberration correction with the catheter hydrophone, clots were mounted centrally within the skullcap such that geometric focus was approximately within the center of the clot. Using phased steering, the focus of the array was steered through a 20 mm diameter spherical, hexagonal-closed-packed (HCP) lattice pattern. The lattice focal point spacing was set to 1.5 mm ($\lambda/2$). This corresponded to 1,749 discrete treatment points. A total of 200 pulses at a peak-negative pressure of 36 MPa were applied to each focal point at an overall PRF of 200 Hz and local PRF of ~0.5 Hz. The total clot volume liquefied with histotripsy was drained by inserting the catheter hydrophone into the clot, removing the hydrophone and aspirating the liquefied volume using a 10 mL syringe. To ensure the reported drainage volumes corresponded to that resulting from histotripsy treatment, 3 control clots, unexposed to histotripsy were drained using the same technique. The lesions of undrained clots treated with histotripsy were analyzed using B-mode ultrasound and T2-weighted MRI. Drained clots were fixed in 10% phosphate buffered formalin (Sigma-Aldrich, St. Louis, MO, USA) and imaged using a DSLR camera (Canon, Tokyo, Japan).

III. Results

A. Hydrophone Characterization

Noise Characterization—An average SNR was obtained by averaging the SNR for each of the 256 single element waveforms measured with the catheter hydrophone. The mean SNR was 36.9 ± 12.7 dB. Fig. 3 shows the noise floor and an unfiltered single element waveform measured using the catheter hydrophone. The key features of the waveform, including the peak-negative signal, were well above the noise floor and able to be distinguished. The average insertion loss of the catheter across all 256 waveforms was −14.0 ± 4.2 dB.

Time-of-flight Measurements and Directivity—To understand how the time-of-flight of the peak-negative pressure measured by our catheter hydrophone varied with the direction of ultrasound propagation from the array, the peak-negative pressure time-of-flight measured by the catheter hydrophone (without the catheter sheath) was compared to that measured with a PVDF capsule hydrophone (Fig. 4). The catheter sheath was excluded from these measurements because the catheter hydrophone could not be accurately rotated 180° in the catheter sheath with our current setup. The reported angular dependent delays were inherent the custom hydrophone in the absence of the sheath. The capsule hydrophone measured a flat time-of-flight around 110.5 μs across all angular positions of ultrasound propagation from the array. In contrast, the catheter hydrophone showed a deviation from this in that the time-of-flight varied with the angular position. The time-of-flight between 100° and 300° gradually increased from 110.5 μs at 100°, peaked around 112.5 μs at 200° and gradually decreased back to 110.5 μs at 300°. A set of angular dependent delays was calculated by subtracting the catheter hydrophone measured peak-negative pressure time-of-flight from that of the capsule hydrophone (Fig. 4c). To ensure this variation in time-of-flight was not a result of a discrepancy in position relative to the capsule hydrophone but rather a characteristic inherent to the catheter hydrophone, the catheter hydrophone was rotated 180° with respect to the array and measurements were repeated. The result was an approximate 180° shift in the angular position at which the peak offset occurred (Fig. 4d).

B. Aberration Correction

An aberration correction algorithm was designed to calculate the delays necessary to realign the peak-negative pressure of the 256 waveforms delivered through the skull. Fig. 5 shows 3 waveforms delivered through the skullcap measured with the catheter hydrophone. There was a noticeable variation in the peak-negative signal time-of-flight among the elements. The waveform delivered from element A had a peak-negative signal that arrived 0.5 μs earlier than that of the reference element. Whereas, the waveform delivered from element B arrived 1.2 μs later than that of the reference element. 10% of the waveforms fell outside the 4 μs window and were readjusted. The relative differences in the time-of-flight among the 256 elements were extracted as the aberration correction delays and uploaded to the FPGA boards.

C. Evaluation of Catheter Hydrophone Aberration Correction

Focal Pressure Measurements—There was a noticeable similarity in plotting the delays calculated with the aberration correction algorithm versus those expected based on the thickness and sound speed of the specific skullcap used in this study (Fig. 6a). Uploading the delays obtained with the catheter hydrophone corresponded to a 60% increase in the peak-negative pressure at the point where aberration correction was performed relative to the no aberration correction case (Fig. 6b). A comparison between focal waveforms after aberration correction performed with a commercial PVDF capsule hydrophone and catheter hydrophone (Fig. 7) showed a 95% increase in the peak-negative pressure by the commercial hydrophone over the case without aberration correction and a 35% increase over the case with the catheter hydrophone aberration correction.

Beam Profiles—To characterize the refocusing effects of catheter hydrophone aberration correction, sagittal, coronal and axial beam profiles were obtained in the absence of aberration and through the skullcap with and without aberration correction (Fig. 8). For all three axes, catheter hydrophone aberration correction sharpened the main lobe of the beam profiles relative to those obtained without aberration correction. Aberration correction also reduced the amplitude of the largest side lobes present without aberration correction. This lead to a reduction in the −6 dB beam width along the sagittal and axial axes to values closer to that obtained with the absence of aberration (Tab. 1). After aberration correction, the −6 dB beam widths in each dimension were within 1.5 mm of their respective width with the absence of aberration compared to 5 mm without aberration correction.

Pressure vs. Electronic Focal Steering—After performing aberration correction at *only* the geometric origin of the array, the focus was steered to a range of positions along the sagittal, coronal and axial axes within the skullcap using phased steering. The peak-negative pressure at each steering location was measured. The normalized peak-negative pressure as a function of transcranial steering position with no aberration and with and without aberration correction is shown in Fig. 9. The increase at the point where aberration correction was performed (i.e., geometric focus) was 60%. Table 2 shows percentage change in the peak-negative pressure for each steering direction. For the coronal and axial axes, the peak-negative pressure measured with aberration correction remained greater than or equal to that measured without aberration correction across the entire steering range examined. In the coronal direction the largest peak-negative pressure increase (62%) was observed +1 mm from the point where aberration correction was performed. For the sagittal axis, the peak-negative pressure measured with aberration correction remained greater than or equal to that measured without aberration correction across a range of −18 to 14 mm. Beyond this range (−19 to −20 mm and 15 to 20 mm), the peak-negative pressure measured with aberration correction was less than that measured without aberration correction. The no aberration case showed pressure losses to a lesser degree at far steering radii than either case with aberration.

Lesion Generation using Electronic Focal Steering—Catheter hydrophone aberration correction was performed at a single point and lesions were generated at discrete electronic steering locations in an RBC phantom positioned within the skullcap. Fig. 10a

shows a 10 × 10 mm grid of transcranial lesions generated after single point aberration correction. Lesions were generated at nearly each point within the 9 × 9 grid with larger and distinct lesions closer to the center and smaller, indistinct lesions toward the corners of the grid beyond 10 mm from the geometric focus. The legion diameter was largest at the geometric origin of the array, where aberration correction was performed, and decreased as the steering distance increased. The diameter of the lesion generated at the geometric focus and the aberration correction point was 1.3 mm. Along the sagittal axis, the lesion diameter decreased to 0.84 and 0.74 mm at the respective negative and positive extremes of the grid (−10 and 10 mm) (Fig. 10b). Along the coronal axis, the lesion diameter decreased to 0.40 and 0.24 mm at the respective positive and negative extremes of the grid (−10 and 10 mm) (Fig. 10c).

In-vitro Clot Treatment using Electronic Focal Steering—Catheter hydrophone aberration correction was performed at a single point and transcranial histotripsy was applied with electronic focal steering. Posttreatment B-mode ultrasound and T2-weighted MR images of the sagittal-coronal plane showed a well-defined lesion in the center of the clot (Fig. 11). The ultrasound image showed a dark, circular contiguous lesion that measured approximately 12 mm in diameter. Similarly, the MR image showed a dense bright contiguous core lesion that was similar in diameter. However, the MR image also showed bright, partially treated blotches of lysed clot beyond this dense core that filled the entirety of the treatment region (i.e., 20 mm diameter). Following treatment, the miniature hydrophone was removed from the catheter and used to drain the liquefied volume. Fig. 12 shows the gross morphology of a treated clot after draining the liquefied volume. A total of six clots were treated and drained within about 30 minutes. The average volume drained from 6 clots after histotripsy treatment was 4.07 ± 0.91 mL. This corresponded well to the 20 mm diameter scanned volume of 4.19 mL. The treatment rate was 0.13 mL/min.

IV. Discussion

The catheter hydrophone used to correct the skull-induced aberration for transcranial histotripsy represents a fast (~10-minute correction time) and minimally invasive mechanism of correcting aberrations for future *in-vivo* application. Particularly for ICH treatment, a drainage catheter is needed to drain the liquefied clot. A miniature hydrophone incorporated within the catheter can overcome the need for MRI-based aberration correction, which MRgFUS currently relies on, and has the potential to significantly simplify the process of aberration correction for transcranial histotripsy treatment of ICH. The results in this paper demonstrate the proof-of-concept and feasibility of catheter hydrophone aberration correction for transcranial histotripsy treatment of ICH. Using the catheter hydrophone, aberration correction was performed at a single point to increase the peak-negative pressure by 60% and sharpen main lobe of the beam. The feasibility for precise histotripsy treatment after single point aberration correction with the catheter hydrophone was demonstrated by the increased peak-negative pressure and discrete lesion formation across a range of electronic steering locations, with no significant damage outside the focal zone. The *in-vitro* clot experiments performed in this study showed the ability to perform catheter hydrophone aberration correction, apply transcranial histotripsy treatment to a

volume of clot, and then drain the liquefied volume with the catheter. This can be achieved an order magnitude faster than the current minimally invasive catheter techniques using thrombolytic drugs [15]. However, it is slightly less than the treatment rate reported with MRgFUS (~0.2 mL/min) [24-26]. This is primarily because the array was driven with a low-pressure overhead (i.e., 36 MPa, 10 MPa over the intrinsic threshold) and enough pulses to completely liquefy the treatment region. This is not entirely necessary in order to drain the treated region with a catheter. In a study recently accepted for publication, we show liquefaction rates of about 3.5 mL/min using greater pressure (70 MPa) and fewer pulses (50) [45].

Low SNR was an issue with early iterations of the catheter hydrophone prototypes that made distinguishing the ultrasound waveforms measured through the skull difficult. This caused calculation errors when using the peak-negative signal of the measurements to deduce the relative delays among the 256 single element waveforms. However, this issue was significantly improved by incorporating a shielded coaxial cable. The version of the custom hydrophone used in this study had sufficient SNR to distinguish the peak-negative pressure from the waveform of each individual element and thus provided a reference point by which to calculate the relative delays. One concern is that using a full human skull will cause a multiplicity of echoes and may disrupt aberration correction. However, proper windowing of the acquisition time will allow such echoes to be excluded from consideration. Assuming the hydrophone tip is sufficiently far from any portion of the skull surface, the time of arrival versus the echo time should be sufficiently far apart for minimal measurement issues.

As the range of clot sizes for ICH varies, histotripsy volume treatment is an important aspect of successful ICH treatment. By performing catheter hydrophone aberration correction at a single point, it was possible to increase the peak-negative pressure across a range of steered locations away from the point at which the aberration correction measurements were acquired, allowing treatment using electronic focal steering. The overall pressure loss as the focus is steered to greater distances is an inherent quality of electronic focal steering and was observed even in the case with no aberration. However, the absence of the skullcap showed losses to a lesser degree. Single point aberration correction may be sufficient for treating ICH cases where the clot boundaries are within the steering range at which pressures are above the intrinsic threshold. This range is a function of pressure applied to the geometric focus. Still, while aberration correction with the catheter hydrophone at a single point led to increased pressures in the bulk of the steered-through volume compared to the no aberration correction case, at steering locations far from the aberration correction point, there was a decreased peak-negative pressure compared to the no aberration correction case. Similar effects to these were seen by Vignon et al. where the improvement in corrective delays acquired from a single point became worse than the uncorrected case at steering angles greater than 30° [74]. However, these effects were attributed to a conversion to shear waves at incidence angles greater than 30°, which the correction did not account for [76]. Due to the hemispherical shape of the array used here, the max incidence angle was on the order of about 8° and shear wave conversion at larger steering angles was likely not a factor. Instead, two factors likely accounted for this: (1) refractive effects and (2) the change in skull thickness through which each pulse propagates en route to the steered-to location. In regards to the first, while refractive deviations to the pulse trajectories are not expected to

significantly contribute to aberration of pulses steered near the origin, this may not be the case at larger steering radii. This is because as the steering radius is increased, the incidence angles of the pulses with the skull's surface can change significantly enough to affect their post-skull trajectories and thus the potential for misalignment at large steering radii. It should be noted, however, that due to the short pulse duration and the necessity of constructive interference to reach the intrinsic threshold, this effect is unlikely to generate off target damage as the tendency toward deconstructive interference would drop the pressure below the intrinsic threshold. We are currently developing an aberration correction algorithm that uses measurements at multiple points along the axis of insertion (i.e., the axis along which the catheter is inserted) to account for refraction effects, which may increase the pressure at a farther steering locations.

In regards to the second factor, as the trajectories of the pulses within the skull change, the path lengths through bone which each pulse must travel also changes, which causes additional misalignment between the pulses as the steering angle increases away from the measurement location. As pulses are aligned at the geometric origin after initial aberration correction, such misalignment can only result in deconstructive interference between the pulses as the focus is steered, and thus lower the pressure. However, in the no aberration correction case, the innate, uncorrected aberration can reduce the magnitude of the losses generated by the additional misalignment due to steering and result in higher pressure amplitudes than with aberration correction. A similar discussion regarding differing propagation paths is proposed by Lindsey and Smith, where steering a 2D imaging probe 15° through skull bone showed decreased correlation of the steered wavefront arrival between adjacent elements on the imaging array [75]. We are currently investigating 1) how much this effect contributes to the observed results, 2) the farthest limit of steering locations beyond which aberration correction reduces the pressure even with multi-location measurements, and 3) methods of correcting for potential losses due to it.

Although the catheter hydrophone used in this study was sufficient to measure the waveforms through the skull, fit within a catheter, and improve the focusing through the skull, there was some deviation in its performance when compared to the PVDF capsule hydrophone. Using the capsule hydrophone with the same correction algorithm showed a 95% increase in the peak-negative pressure at the geometric origin through the skullcap used in this study (a 35% greater increase over the catheter hydrophone). Since this measurement is a metric on how well the individual waveforms were temporally aligned using time-of-flight measurements made with each hydrophone, it is likely that the deviation in performance in relation to the capsule hydrophone was likely due to the angular dependent delay in the time-of-flight measurements of individual waveforms made with the catheter hydrophone.

One additional comment is that as this study used an excised human skullcap instead of a full human skull, it was possible to insert the catheter hydrophone into the open end of the skullcap. Although this orientation sufficed for showing the proof-of-concept, this insertion trajectory is not likely in a clinical setting where catheters are often inserted through small holes drilled through the skullcap. An ideal catheter hydrophone insertion strategy would involve removing an element from the array overlying the hole drilled for access to the clot

and guiding the catheter hydrophone through the hole in the array into the skull. This flipped insertion strategy is likely to affect the quality of signal acquisition as it the flips the orientation of the device such that the coaxial cable and catheter interfere with the propagation path from a number of elements. However, any amplitude or phase distortion can likely be overcome using an edge detection correction technique. As our histotripsy array is made with each element as a removable module, we plan to build a catheter holder that can be easily fitted through each element module opening. This would allow a large range of possible entrance points into the skull for a large range of clot locations. Future in-vitro experiments will use full human skulls with a small hole drilled into the skullcap for inserting the catheter hydrophone.

V. Conclusion

The purpose of this study was to establish the proof-of-concept for using catheter hydrophone aberration correction as an aberration correction technique in the development of histotripsy as a minimally invasive technology for treating ICH. A custom miniature hydrophone was integrated with a drainage catheter. A time delay based aberration correction algorithm was developed to allow aberration correction using the catheter hydrophone measurements at a single location. The catheter hydrophone was characterized and the functionality of using catheter hydrophone measurements to perform aberration correction was measured. Finally, an *in-vitro* study was conducted to demonstrate the proof-of-concept of using the catheter hydrophone for clot liquefaction and drainage through an excised human skullcap. This study exemplified the potential of such a device to be used for future *in-vivo* studies and clinical applications of minimally invasive treatment for ICH using transcranial histotripsy. Future work includes examining the potential for angular dependence in time-of-flight measurements, establishing a catheter insertion strategy, and developing a catheter array with associated aberration correction algorithm that uses measurements at multiple points to potentially increase the electronic focal steering range.

Acknowledgments

The authors would like to thank the Anatomical Donations Program at the University of Michigan for providing the skull samples used in this study.

This work was supported by grants from the National Institute of Neurological Disorders and Stroke (NINDS) of the National Institutes of Health (NIH) under Award Number R21-NS093121, the National Institute of Biomedical Imaging and Bioengineering (NIBIB) of the NIH under Award Number R01-EB008998 and the National Science Foundation Graduate Research Fellowship Program under Grant No. (2017239378).

Biographies

Tyler Gerhardson is a graduate student in the Department of Biomedical Engineering at the University of Michigan, Ann Arbor, MI, USA. He received a B.S. degree in biomedical engineering from Western New England University, Springfield, MA, USA in 2015 and an M.S. Degree in biomedical engineering from the University of Michigan in 2017. Selected honors include the Deans Award for Academic Excellence and Biomedical Engineering Department Award for Outstanding Senior from Western New England University, a Scholarship and Fellowship from Tau Beta Pi and a National Science Foundation Graduate Research Fellowship. Tyler's research interests include ultrasonic standing wave separators, ultrasound transducers and focused ultrasound therapies.

Jonathan R. Sukovich received the B.S. and Ph.D. degrees in mechanical engineering from Boston University, Boston, MA, USA, in 2008 and 2013, respectively, where he studied laser interactions with water at high pressures and phenomena associated with high-energy bubble collapse events.

He is a research scientist with the Department of Biomedical Engineering, University of Michigan, Ann, MI, USA. He joined the University of Michigan in the summer of 2013 to study histotripsy for brain applications. His research interests include high-energy bubble collapse phenomena, focused ultrasound therapies, and acoustic cavitation.

Aditya S. Pandey received the B.Sc. degree in biological and engineering sciences from Washington University in St. Louis, MO, USA, and the Doctorate of Medicine from Case Western Reserve University School of Medicine, Cleveland, OH, USA, in 1997 and 2001, respectively.

He then gained training in neurological surgery with subspecialty training in microsurgical and endovascular treatment of cerebrovascular disorders. He specializes in treating individuals who have blood vessel-related diseases of the brain and spinal cord (e.g., aneurysms, AVM, stroke, fistulas, and cavernomas) as well as practicing general neurosurgery (spinal disorders, brain tumors, and traumatic brain injury). He is one of two neurosurgeons in the Ann Arbor region who are trained to perform both open surgeries and

endovascular radiological procedures when treating brain blood vessel-related diseases. He has authored more than 30 research publications as well as participated in numerous national research trials aimed at improving techniques of aneurysm treatment. He is currently leading a study to better understand whether a patient requiring aneurysm treatment should be maintained on seizure medications post-surgery. His research interests include developing and improving tools to assist in the fight against stroke and brain aneurysms.

Timothy L. Hall was born in Lansing, MI, USA, in 1975. He received the B.S.E. and M.S.E. degrees in electrical engineering, and the Ph.D. degree in biomedical engineering, all from the University of Michigan, Ann Arbor, MI, USA, in 1998, 2001, and 2007, respectively. He is currently an Assistant Research Scientist with the Department of Biomedical Engineering, University of Michigan. He worked with Teradyne Inc., Boston, MA, USA, from 1998 to 1999, as a Circuit Design Engineer and with the University of Michigan, from 2001 to 2004, as a Visiting Research Investigator. His research interests include high-power pulsed-RF-amplifier electronics, phased-array ultrasound transducers for therapeutics, and sonic cavitation for therapeutic applications.

Charles A. Cain S′65–M′71–SM′80–F′89) was born in Tampa, FL, USA, on March 3, 1943. He received the B.E.E. (highest hons.) degree from the University of Florida, Gainesville, FL, USA, in 1965, the M.S.E.E. degree from the Massachusetts Institute of Technology, Cambridge, MA, USA, in 1966, and the Ph.D. degree in electrical engineering from the University of Michigan, Ann Arbor, MI, USA, in 1972. From 1965 through 1968, he was a Member of the Technical Staff with Bell Laboratories, Naperville, IL, USA, where he worked in the electronic switching systems development area. From 1972 through 1989, he was with the Department of Electrical and Computer Engineering, University of Illinois at Urbana–Champaign, Champaign, IL, USA, where he was a Professor of Electrical Engineering and Bioengineering. Since 1989, he has been with the College of Engineering, University of Michigan, as a Professor of Biomedical Engineering and Electrical Engineering. He was the Chair of the Biomedical Engineering Program from 1989 to 1996, the Founding Chair of the Biomedical Engineering Department from 1996 to 1999, and the

Richard A. Auhll Professor of Engineering in 2002. He has been involved in research on the medical applications of ultrasound, particularly high-intensity ultrasound for noninvasive surgery.

Dr. Cain was formerly an Associate Editor of the IEEE TRANSACTIONS ON BIOMEDICAL ENGINEERING and the IEEE TRANSACTIONS ON ULTRASONICS, FERROELECTRICS, AND FREQUENCY CONTROL, and an Editorial Board Member of the International Journal of Hyperthermia and Radiation Research. He is a Fellow the American Institute for Medical and Biological Engineering (AIMBE).

Zhen Xu (S′05–M′06) received the B.S.E. (highest hons.) degree from Southeast University, Nanjing, China, in 2001, and the M.S. and Ph.D. degrees from the University of Michigan, Ann Arbor, MI, USA, in 2003 and 2005, respectively, all in biomedical engineering. She is an Associate Professor with the Department of Biomedical Engineering, University of Michigan. Her research interests include ultrasound therapy, particularly the applications of histotripsy for noninvasive surgeries. Dr. Xu is currently an Associated Editor for the IEEE TRANSACTIONS ON ULTRASONICS, FERROELECTRICS, AND FREQUENCY CONTROL (UFFC), Women In Engineering (WIE) chair for UFFC, and board member of the International Society of Therapeutic Ultrasound (ISTU). She received the UFFC Outstanding Paper Award in 2006; the American Heart Association (AHA) Outstanding Research in Pediatric Cardiology in 2010; the National Institute of Health (NIH) New Investigator Award at the First National Institute of Biomedical Imaging and Bioengineering (NIBIB) Edward C. Nagy New Investigator Symposium in 2011; and the Frederic Lizzi Early Career Award from ISTU in 2015.

References

1. Qureshi AI, Mendelow AD, Hanley DF. Intracerebral haemorrhage. Lancet. May; 2009 373(9675): 1632–1644. [PubMed: 19427958]
2. Mozaffarian D, Benjamin EJ, Go AS, Arnett DK, Blaha MJ, Cushman M, Das SR, de Ferranti S, Després J-P, Fullerton HJ, Howard VJ, Huffman MD, Isasi CR, Jiménez MC, Judd SE, Kissela BM, Lichtman JH, Lisabeth LD, Liu S, Mackey RH, Magid DJ, McGuire DK, Mohler ER, Moy CS, Muntner P, Mussolino ME, Nasir K, Neumar RW, Nichol G, Palaniappan L, Pandey DK, Reeves MJ, Rodriquez CJ, Rosamond W, Sorlie PD, Stein J, Towfighi A, Turan TN, Virani SS, Woo D, Yeh RW, Turner MB. Executive summary: heart disease and stroke statistics—2016 update: a report from the American Heart Association. Circ. Jan; 2016 133(4):447–454.
3. Kuklina EV, Tong X, George MG, Bansil P. Epidemiology and prevention of stroke: a worldwide perspective. Expert Rev Neurother. Feb; 2012 12(2):199–208. [PubMed: 22288675]
4. Flaherty ML, Haverbusch M, Sekar P, Kissela B, Kleindorfer D, Moomaw CJ, Sauerebeck L, Schneider A, Broderick JP, Woo D. Long-term mortality after intracerebral hemorrhage. Neurology. Apr; 2006 66(8):1182–1186. [PubMed: 16636234]

5. Broderick JP, Brott TG, Duldner JE, Tomsick T, Huster G. Volume of intracerebral hemorrhage. A powerful and easy-to-use predictor of 30-day mortality. Stroke. Mar; 1993 24(7):987–993. [PubMed: 8322400]
6. Rincon F, Mayer SA. Clinical review: critical care management of spontaneous intracerebral hemorrhage. Crit Care. Dec; 2008 12(6):237–251. [PubMed: 19108704]
7. Skidmore CT, Andrefsky J. Spontaneous intracerebral hemorrhage: epidemiology, pathophysiology, and medical management. Neurosurg Clin N Am. Jul; 2002 13(3):281–288. [PubMed: 12486918]
8. Gujjar AR, Deibert E, Manno EM, Duff S, Diringer MN. Mechanical ventilation for ischemic stroke and intracerebral hemorrhage: indications, timing and outcome. Neurol. Aug; 1998 51(2):447–451.
9. Diringer MN. Intracerebral hemorrhage: pathophysiology and management. Crit Care. Oct; 1993 21(10):1591–1603.
10. Hankey GJ, Hon C. Surgery for primary intracerebral hemorrhage: is it safe and effective? A systematic review of case series and randomized trials. Stroke. Aug; 1997 28(11):2126–2132. [PubMed: 9368552]
11. Fernandes HM, Gregson B, Siddique S, Mendelow AD. Surgery in intracerebral hemorrhage the uncertainty continues. Stroke. Oct; 2000 31(10):2511–2516. [PubMed: 11022087]
12. Mendelow AD, Gregson BA, Fernandes HM, Murray GD, Teasdale GM, THope D, Karimi A, Shaw MD, Barer DH. Early surgery versus initial conservative treatment in patients with spontaneous supratentorial intracerebral haematomas in the Internation Surgical Trial in Intracerebral Haemorrhage (STICH): a randomised trial. Lancet. Jan; 2005 365(9457):387–397. [PubMed: 15680453]
13. Mendelow AD, Gregson BA, Rowan EN, Murray GD, Gholkar A, Mitchell PM. Early surgery versus initial conservative treatment in patients with spontaneous supratentorial lobar intracerebral haematomas (STICH II): a randomised trial. Lancet. Aug; 2013 382(9890):397–408. [PubMed: 23726393]
14. Hattori N, Katayama Y, Maya Y, Gaherer A. Impact of stereotactic hematoma evacuation on medical costs during the chronic period in patients with spontaneous putaminal hemorrhage: a randomized study. Surg Neurol. May; 2006 65(5):429–435. [PubMed: 16630899]
15. Morgan T, Zuccarello M, Narayan R, Keyl P, Lane K, Hanley D. Preliminary findings of the minimally-invasive surgery plus rtPA for intracerebral hemorrhage evacuation (MSITIE) clinical trial. Acta Neurochir Suppl. 2008; 105:147–151. [PubMed: 19066101]
16. Wang WZ, Jiang B, Liu HM, Li D, Lu CZ, Zhao YD, Sander JW. Minimally invasive craniopuncture therapy vs. conservative treatment for spontaneous intracerebral hemorrhage: results from a randomized clinical trial in China. Int J Stroke. Feb; 2009 4(1):11–16. [PubMed: 19236490]
17. Alexandrov AV, Demchuk AM, Burgin WS, Robinson DJ, Grotta JC. Ultrasound-enhanced thrombolysis for acute ischemic stroke: Phase i. findings of the clotbust trial. J Neuroimaging. Apr; 2004 14(2):113–117. [PubMed: 15095555]
18. Datta S, Coussios C-C, McAdory LE, Tan J, Porter T, De Courten-Myers G, Holland CK. Correlation of cavitation with ultrasound enhancement of thrombolysis. Ultrasound Med Biol. Aug; 2006 32(8):1257–1267. [PubMed: 16875959]
19. Datta S, Coussios C-C, Ammi AY, Mast TD, de Courten-Myers GM, Holland CK. Ultrasound-enhanced thrombolysis using definity®as a cavitation nucleation agent. Ultrasound Med Biol. Sep; 2008 34(9):1421–1433. [PubMed: 18378380]
20. Alexandrov AV, Mikulik R, Ribo M, Sharma VK, Lao AY, Tsivgoulis G, Sugg RM, Barreto A, Sierzenski P, Malkoff MD, Grotta JC. A pilot randomized clinical safety study of sonothrombolysis augmentation with ultrasound-activated perflutren-lipid microspheres for acute ischemic stroke. Stroke. May; 2008 39(5):1464–1469. [PubMed: 18356546]
21. Holland CK, Vaidya SS, Datta S, Coussios C-C, Shaw GJ. Ultrasound-enhanced tissue plasminogen activator thrombolysis in an in vitro porcine clot model. Thromb Res. 2008; 121(5): 663–673. [PubMed: 17854867]
22. Hitchcock KE, Holland CK. Ultrasound-assisted thrombolysis for stroke therapy better thrombus break-up with bubbles. Stroke. Oct; 2010 41(10):S50–S53. [PubMed: 20876505]

23. Meairs S, Alonso A, Hennerici MG. Progress in sonothrombolysis for the treatment of stroke. Stroke. Jun.2012 43:1706–1710. [PubMed: 22535275]
24. Monteith SJ, Harnof S, Medel R, Popp B, Wintermark M, Lopes MB, Kassel NF, Elias WJ, Snell J, Eames M, Zadicario E, Moldovan K, Sheehan J. Minimally invasive treatment of intracerebral hemorrhage with magnetic resonance-guide focused ultrasound. J Neurosurg. May; 2013 118(5): 1035–1045. [PubMed: 23330996]
25. Monteith SJ, Kassell NF, Goren O, Harnof S. Transcranial MR-guided focused ultrasound sonothrombolysis in the treatment of intracerebral hemorrhage. Neurosurg Focus. May.2013 34(5)
26. Ramanan M, Shankar A. Minimally invasive surgery for primary supratentorial intracerebral haemorrhage. J Clin Neurosci. Dec; 2013 20(12):1650–1658. [PubMed: 24161339]
27. Monteith S, Sheehan J, Medel R, Wintermark M, Eames M, Snell J, Kassell NF, Elias WJ. Potential intracranial applications of magnetic resonance-guided focused ultrasound surgery. J Neurosurg. Feb; 2013 118(2):215–221. [PubMed: 23176339]
28. Wright C, Hynynen K, Goertz D. In vitro in vivo high-intensity focused ultrasound thrombolysis. Invest Radiol. Apr; 2012 47(4):217–225. [PubMed: 22373533]
29. Elias WJ, Huss D, Voss T, Loomba J, Khaled M, Frysinger RC, Sperling S, Wylie S, Monteith S, Druzgal J, Shah B, Harrison M, Wintermark M. The use of magnetic resonance-guided high intensity focused ultrasound to treat essential tremor. J Acoust Soc Am. 2013; 134(5):4090.
30. Xu Z, Ludomirsky A, Eun LY, Hall TL, Tran BC, Folkes JB, Cain CA. Controlled ultrasound tissue erosion. IEEE Trans Ultrason Ferroelectr Freq Control. Jun; 2004 51(6):726–736. [PubMed: 15244286]
31. Xu Z, Folkes JB, Rothman ED, Levin AM, Cain CA. Controlled ultrasound tissue erosion: the role of dynamic interaction between insonation microbubble activity. J Acoust Soc Am. Jan; 2005 117(1):242–435.
32. Roberts WW, Hall TL, Ives K, Wolf JS Jr, Fowlkes JB, Cain CA. Pulsed cavitational ultrasound: a noninvasive technology for controlled tissue ablation (histotripsy) in the rabbit kidney. The Journal of Urology. Feb; 2006 175(2):734–738. [PubMed: 16407041]
33. Xu Z, Owens G, Gordon D, Cain CA, Ludomirsky A. Noninvasive creation of an atrial septal defect by histotripsy in a canine model. Circ. Feb; 2010 121(6):742–749.
34. Lin K, Kim Y, Maxwell AD, Wang T, Hall TL, Xu Z, Fowlkes B, Cain CA. Histotripsy beyond the “intrinsic” threshold using very short ultrasound pulses: “microtripsy”. IEEE Trans Ultrason Ferroelectr Freq Control. Feb; 2014 61(2):251–265. [PubMed: 24474132]
35. Maxwell AD, Owens G, Gurm HS, Ives K, Myers DD Jr, Xu Z. Noninvasive treatment of deep venous thrombosis using pulsed ultrasound cavitation therapy (histotripsy) in a porcine model. J Vasc Interv Radiol. Mar; 2011 22(3):369–377. [PubMed: 21194969]
36. Maxwell AD, Cain CA, Duryea AP, Yuan L, Gurm HS, Xu Z. Noninvasive thrombolysis using pulsed ultrasound cavitation therapy – histotripsy. Ultrasound Med Biol. Dec; 2009 35(12):1982–1994. [PubMed: 19854563]
37. Zhang X, Owens GE, Gurm HS, Ding Y, Cain CA, Xu Z. Noninvasive thrombolysis using histotripsy beyond the intrinsic threshold (microtripsy). IEEE Trans Ultrason Ferroelectr Freq Control. Jul; 2015 62(7):1342–1355. [PubMed: 26168180]
38. Zhang X, Jin L, Vlaisavljevich E, Owens GE, Gurm HS, Cain CA, Xu Z. Noninvasive thrombolysis using microtripsy: a parameter study. IEEE Trans Ultrason Ferroelectr Freq Control. Dec; 2015 62(12):2092–2105. [PubMed: 26670850]
39. Zhang X, Owens GE, Cain CA, Gurm HS, Macoskey JJ, Xu Z. Histotripsy thrombolysis on retracted clots. Ultrasound Med Biol. Aug; 2016 42(8):1903–1918. [PubMed: 27166017]
40. Zhang X, Macoskey JJ, Ives K, Owens GE, Gurm HS, Shi J, Pizzuto M, Cain CA, Xu Z. Non-invasive thrombolysis using microtripsy in a porcine deep vein thrombosis model. Ultrasound Med Biol. Jul; 2017 43(7):1378–1390. [PubMed: 28457630]
41. Devanagondi R, Zhang X, Xu Z, Ives K, Levin A, Gurm H, Owens GE. Hemodynamic hematologic effects of histotripsy of free-flowing blood: implications for ultrasound-mediated thrombolysis. J Vasc Interv Radiol. Oct; 2015 26(10):1559–1565. [PubMed: 25952642]

42. Khokhlova TD, Monsky WL, Haider YA, Maxwell AD, Wang Y, Matula TJ. Histotripsy liquefaction of large hematomas. Ultrasound Med Biol. Jul; 2016 42(7):1491–1498. [PubMed: 27126244]
43. Kim Y, Hall TL, Xu Z, Cain CA. Transcranial histotripsy therapy: a feasibility study. IEEE Trans Ultrason Ferroelectr Freq Control. Apr; 2014 61(4):582–593.
44. Sukovich JR, Xu Z, Kim Y, Cao H, Nguyen T-S, Pandey AS, Hall TL, Cain CA. Targeted lesion generation through the skull without aberration correction using histotripsy. IEEE Trans Ultrason Ferroelectr Freq Control. May; 2016 63(5):671–682.
45. Gerhardson T, Sukovich JR, Pandey AS, Hall TL, Cain CA, Xu Z. Effect of frequency focal spacing on transcranial histotripsy clot liquefaction, using electronic focal steering. Ultrasound Med Biol. Oct; 2017 43(10):2302–2317. [PubMed: 28716432]
46. Clement G, Hynynen K. Correlation of ultrasound phase with physical skull properties. Ultrasound Med Biol. May; 2002 28(5):617–624. [PubMed: 12079698]
47. Aubry J-F, Tanter M, Pernot M, Thomas J-L, Fink M. Experimental demonstration of noninvasive transskull adaptive focusing based on prior computed tomography scans. J Acoust Soc Am. Jan; 2003 113(1):84–93. [PubMed: 12558249]
48. Hertzberg Y, Volovick A, Zur Y, Medan Y, Vitek S, Navon G. Ultrasound focusing using magnetic resonance acoustic radiation imaging: Application to ultrasound transcranial therapy. Med Phys. May; 2010 37(6):2934–2942.
49. Zeng X, McGough RJ. Evaluation of the angular spectrum approach for simulations of near-field pressure. J Acoust Soc Am. Jan; 2008 123(1):68–76. [PubMed: 18177139]
50. Clement G, White P, Hynynen K. Enhanced ultrasound transmission through the human skull using shear mode conversion. J Acoust Soc Am. Mar; 2004 115(3):1356–1364. [PubMed: 15058357]
51. Clement G, Hynynen K. A non-invasive method for focusing ultrasound through the human skull. Phys Med Biol. Apr; 2002 47(8):1219–1236. [PubMed: 12030552]
52. Hynynen K, Clement GT, McDannold N, Vykhodtseva N, King R, White PJ, Vitek S, Jolesz FA. 500-element ultrasound phased array system for noninvasive focal surgery of the brain: a preliminary rabbit study with ex vivo human skulls. Magn Reson Med. Jun; 2004 52(1):100–107. [PubMed: 15236372]
53. Marsac L, Chauvet D, Greca RLa, Boch A-L, Chaumoitre K, Tanter M, Aubry J-F. *Ex vivo* optimisation of a heterogeneous speed of sound model of the human skull for non-invasive transcranial focused ultrasound at 1 MHz. Int J Hyperthermia, pp. Mar.2017 :1–11.
54. Marquet F, Pernot M, Aubry J-F, Montaldo G, Marsac L, Tanter M, Fink M. Non-invasive transcranial ultrasound therapy based on a 3D CT scan: protocol validation *in vitro* results. Phys Med Biol. Apr.2009 54(9)
55. Chauvet D, Marsac L, Pernot M, Boch A-L, Guillevin R, Salameh N, Souris L, Darrasse L, Fink M, Tanter M, Aubry J-F. Targeting accuracy of transcranial magnetic resonance-guided high-intensity focused ultrasound brain therapy: a fresh cadaver model. J Neurosurg. May; 2013 118(5): 1046–1052. [PubMed: 23451909]
56. Gateau J, Marsac L, Pernot M, Aubry J-F, Fink M. Transcranial ultrasonic therapy based on time reversal of acoustically induced cavitation bubble signature. IEEE Trans Biomed Eng. Sep; 2009 57(1):134–144. [PubMed: 19770084]
57. Pernot M, Aubry J-F, Tanter M, Boch A-L, Marquet F, Kujas M, Seilhean D, Fink M. In vivo transcranial brain surgery with an ultrasounic time reversal mirror. J Neurosurg. Jun; 2007 106(6): 1061–1066. [PubMed: 17564179]
58. Phillips D, Smith S, Ramm OVon, Thurstone F. Sampled aperture techniques applied to B-mode echoencephalography. Acoust Hologr. 1975; 6:103–120.
59. Flax S, O'Donnell M. Phase-aberration correction using signals from point reflectors diffuse scatterers: basic principles. IEEE Trans Ultrason Ferroelectr Freq Control. Nov; 1988 35(6):758–767. [PubMed: 18290213]
60. Fink MA. Time reversal of ultrasonic field. I. basic principles. IEEE Trans Ultrason Ferroelectrc Freq Control. Sep; 1992 39(5):555–566.

61. Thomas JL, Fink MA. Ultrasonic beam focusing through tissue inhomogeneities with a time reversal mirror: applications to transskull therapy. IEEE Trans Ultrason Ferroelectr Freq Control. Nov; 1996 43(6):1122–1129.
62. Fink M, Montaldo G, Tanter M. Time-reversal acoustics in biomedical engineering. Annu Rev Biomed Eng. Jun.2003 5:465–497. [PubMed: 14527319]
63. Vignon F, Aubry J, Tanter M, Margoum A, Fink M. Adaptive focusing for transcranial ultrasound imaging using dual arrays. J Acoust Soc Am. Aug; 2006 120(1):2737–2745. [PubMed: 17139734]
64. Seip R, VanBaren P, Ebbini ES. Dynamic focusing in ultrasound hyperthermia treatments using implantable hydrophone arrays. IEEE Trans Ultrason Ferroelectr Freq Control. Sep; 1994 41(5): 7016–713.
65. Pernot M, Montaldo G, Tanter M, Fink M. Ultrasonic stars' for time-reversal focusing using induced cavitation bubbles. Appl Phys Lett. Jan.2006 88(3):034102.
66. Haworth KJ, Fowlkes JB, Carson PL, Kripfgans OD. Towards aberration correction of transcranial ultrasound using acoustic droplet vaporization. Ultrasound Med Biol. Mar; 2008 34(3):435–445. [PubMed: 17935872]
67. Maxwell AD, Wang T-Y, Yuan L, Duryea AP, Xu Z, Cain CA. A tissue phantom for visualization measurement of ultrasound-induced cavitation damage. Ultrasound Med Biol. Dec; 2010 36(12): 2132–2143. [PubMed: 21030142]
68. Maxwell AD, Cain CA, Hall TL, Fowlkes JB, Xu Z. Probability of cavitation for single ultrasound pulses applied to tissues tissue-mimicking materials. Ultrasound Med Biol. Mar; 2013 39(3):449–465. [PubMed: 23380152]
69. Wang T-Y, Xu Z, Hall TL, Fowlkes JB, Cain CA. An efficient treatment strategy for histotripsy by removing cavitation memory. Ultrasound Med Biol. May; 2012 38(5):753–766. [PubMed: 22402025]
70. Kim Y, Maxwell AD, Hall TL, Xu Z, Lin K-W, Cain CA. Rapid prototyping fabrication of focused ultrasound transducers. IEEE Trans Ultrason Ferroelectr Freq Control. 2014; 61(9):1559–1574. [PubMed: 25167156]
71. Parsons JE, Cain CA, Fowlkes JB. Cost-effective assembly of a basic fiber-optic hydrophone for measurement of high-amplitude therapeutic ultrasound fields. J Acoust Soc Am. Dec; 2005 119(3):1432–1440.
72. Aguilar MI, Brott TG. Update in intracerebral hemorrhage. Neurohospitalist. Jun; 2013 1(3):148–159.
73. Zimmerman RD, Maldjian JA, Brun NC, Horvath B, Skolnick BE. Radiologic estimation of hematoma volume intracerebral hemorrhage trial by CT scan. Am J Neuroradiol. Mar; 2006 27(3): 666–670. [PubMed: 16552014]
74. Vignon, F., Shi, WT., Burcher, MR., Powers, JE. Determination of temporal bone isoplanatic patch sizes for transcranial phase aberration correction; presented at IEEE International Ultrasonics Symposium; Beijing, China. 2008. p. 1286-1289.
75. Lindsey BD, Smith SW. Pitch-catch phase aberration correction of multiple isoplanatic patches for 3-D transcranial ultrasound imaging. IEEE Trans Ultrason Ferroelectr Freq Control. Mar; 2013 60(3):463–480. [PubMed: 23475914]
76. Pichardo S, Hynynen K. Treatment of near-skull brain tissue with a focused devise using shear-mode conversion: a numerical study. Phys Med Biol. Dec; 2007 52(24):7313–7332. [PubMed: 18065841]
77. Jones RM, Hynynen L. Comparison of analytical numerical approaches for CT-based aberration correction in transcranial passive acoustic imaging. Phys Med Biol. Nov; 2015 61(1):23–36. [PubMed: 26605827]

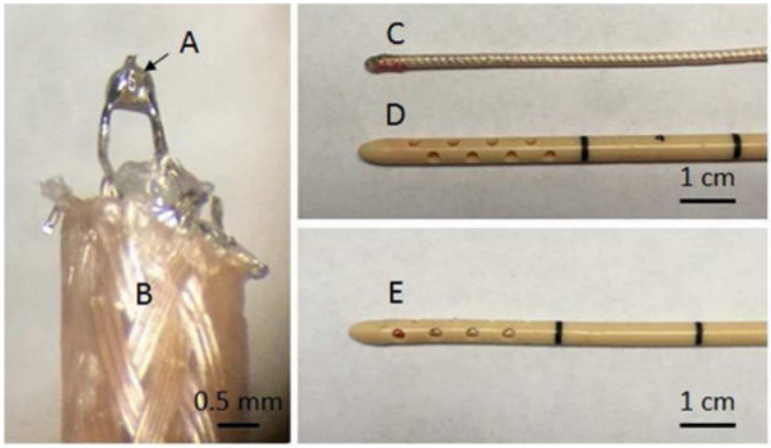

Fig. 1.

Images of the fabrication steps of a custom catheter hydrophone. (A) indicates a 0.5 × 0.5 × 0.3 mm PZT-5 crystal soldered between the leads of a (B) 1.77 mm OD coaxial cable. (C) shows the crystal-cable assembly after coating the tip with epoxy (D) shows the clinical drainage catheter. (E) displays the final assembly of the catheter hydrophone.

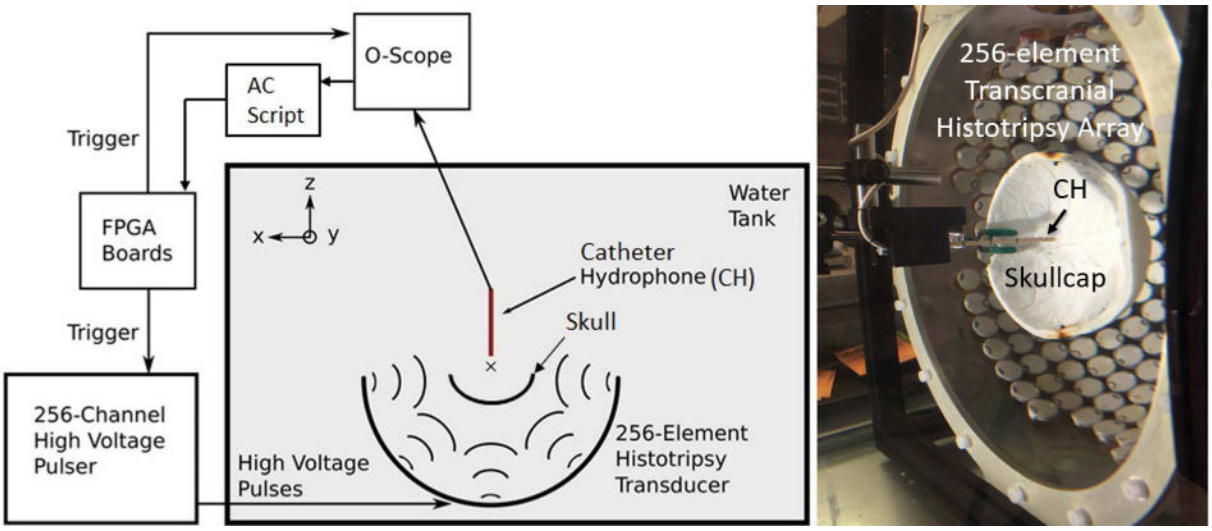

Fig. 2.

The experimental schematic of the setup used to perform the transcranial histotripsy clot treatments through the excised human skullcaps (left) a photograph of the actual experimental setup (right). The 256 individual elements of the array were triggered one-at-a-time, to emit histotripsy pulses. Waveforms were measured by the catheter hydrophone (CH) uploaded to an aberration correction algorithm. The 256 element delays were obtained uploaded to the FPGA boards.

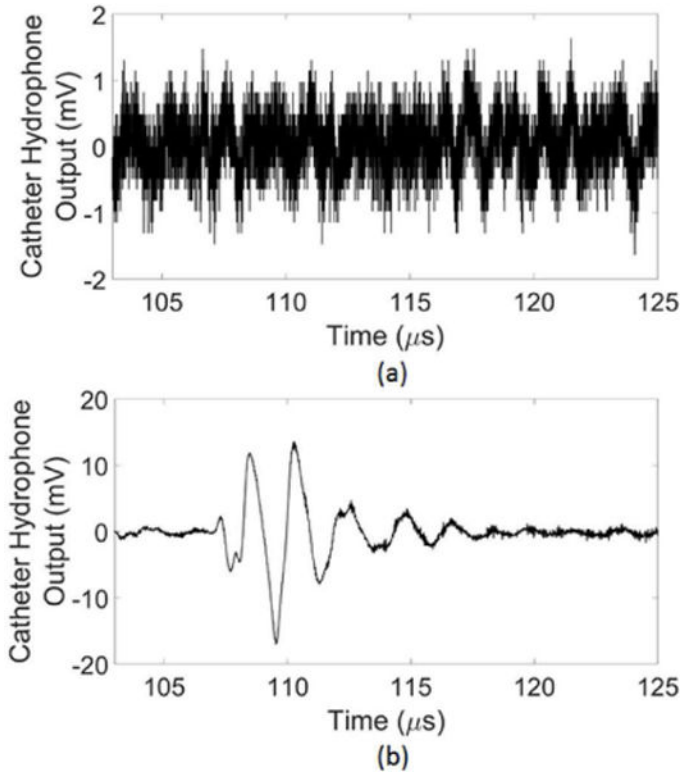

Fig. 3.

(a) The catheter hydrophone noise floor (b) an unfiltered single element waveform measured using the catheter hydrophone.

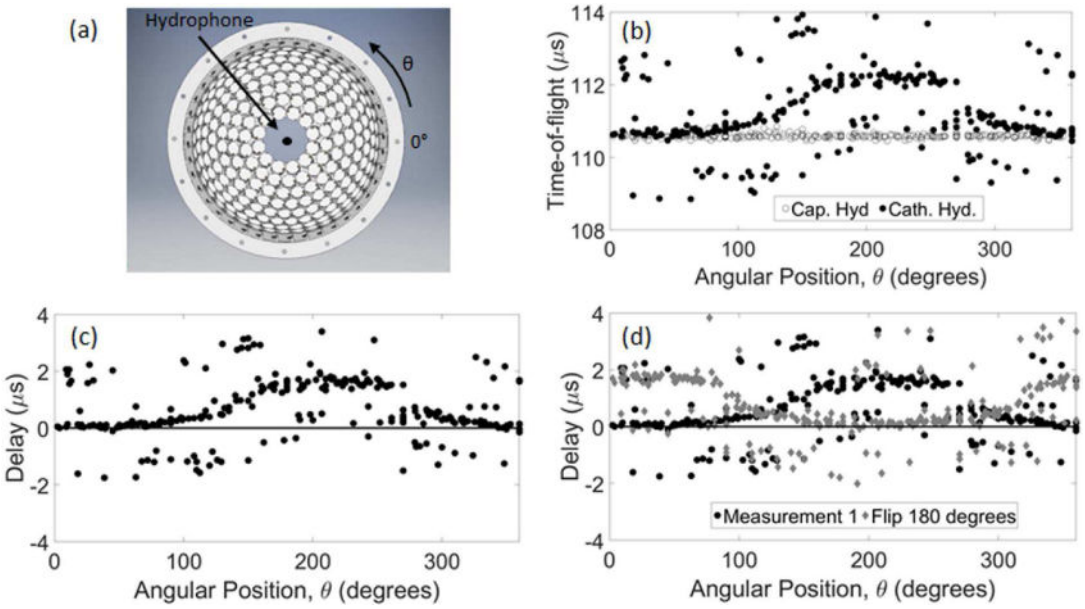

Fig. 4.

The peak-negative pressure time-of-flight measured by the catheter hydrophone (Cath. Hyd.) compared to that measured with a PVDF capsule hydrophone (Cap. Hyd.). (a) shows the position of each hydrophone within the array used to measure the (b) time-of-flight of each waveform. (c) Delays in the catheter hydrophone measurement relative to the capsule hydrophone were calculated by subtracting those measured with the capsule hydrophone. (d) The measurement was repeated after flipping the catheter hydrophone 180° with respect to the array.

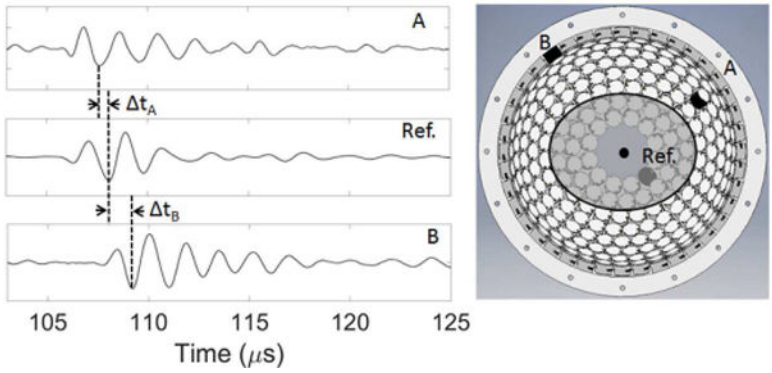

Fig. 5.

Three single element waveforms delivered through the skullcap measured with the catheter hydrophone.

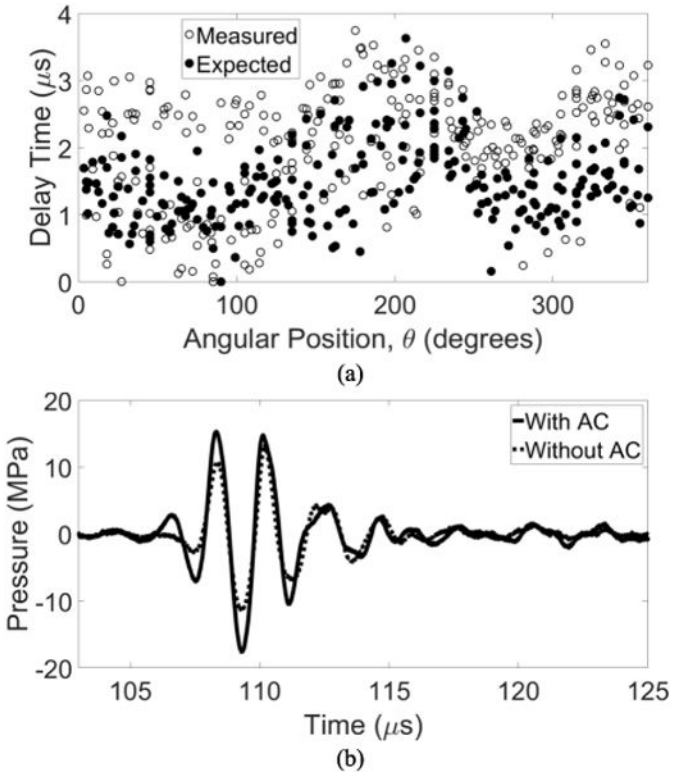

Fig. 6.

(a) Delays obtained via catheter hydrophone aberration correction plotted with those delays expected based on the sound speed thickness of the skullcap used in this study. (b) The focal waveform obtained after implementing aberration correction compared to that without.

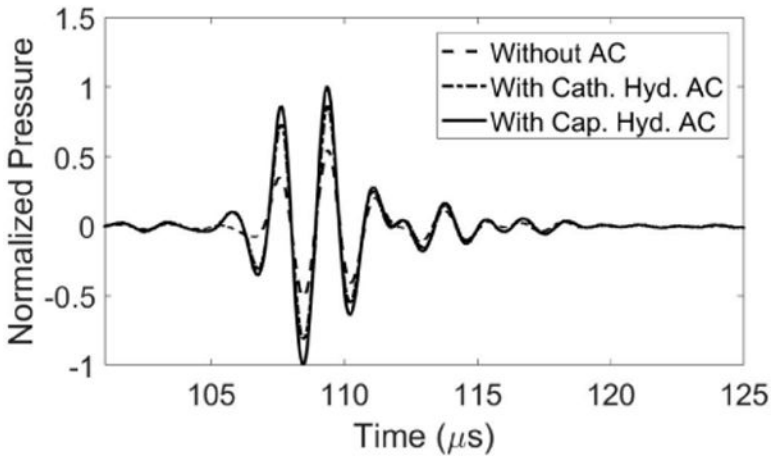

Fig. 7.

Focal waveforms after aberration correction performed with catheter hydrophone (Cath. Hyd.) PVDF capsule hydrophone (Cap. Hyd.) measurements compared to that with no aberration correction.

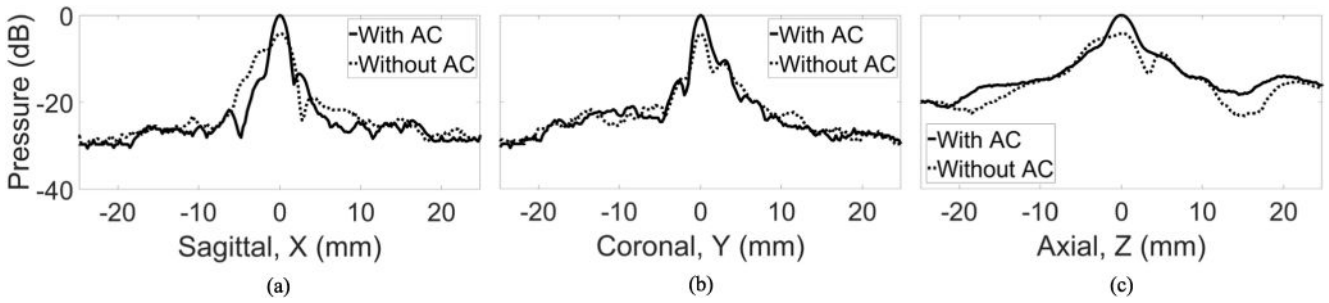

Fig. 8.

The (a) sagittal, (b) coronal (c) axial beam profile measured through the skull with without catheter hydrophone aberration correction (AC).

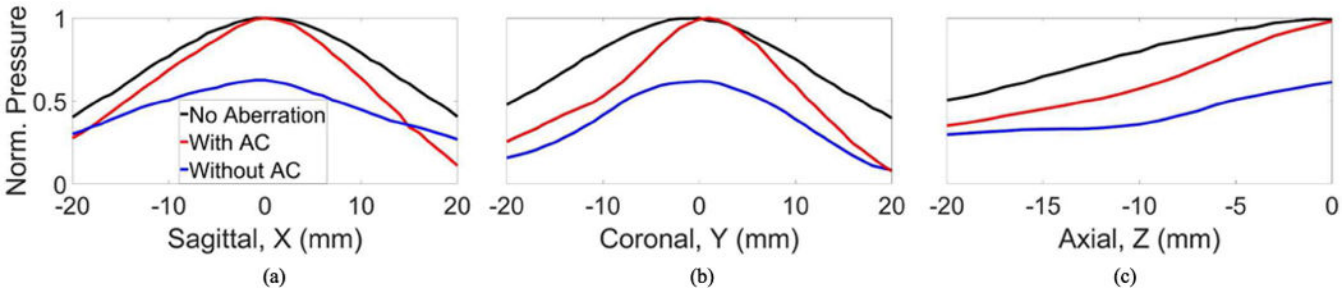

Fig. 9.

The normalized pressure as a function of steering position with no aberration with without aberration correction measured along the (a) sagittal, (b) coronal (c) axial axis.

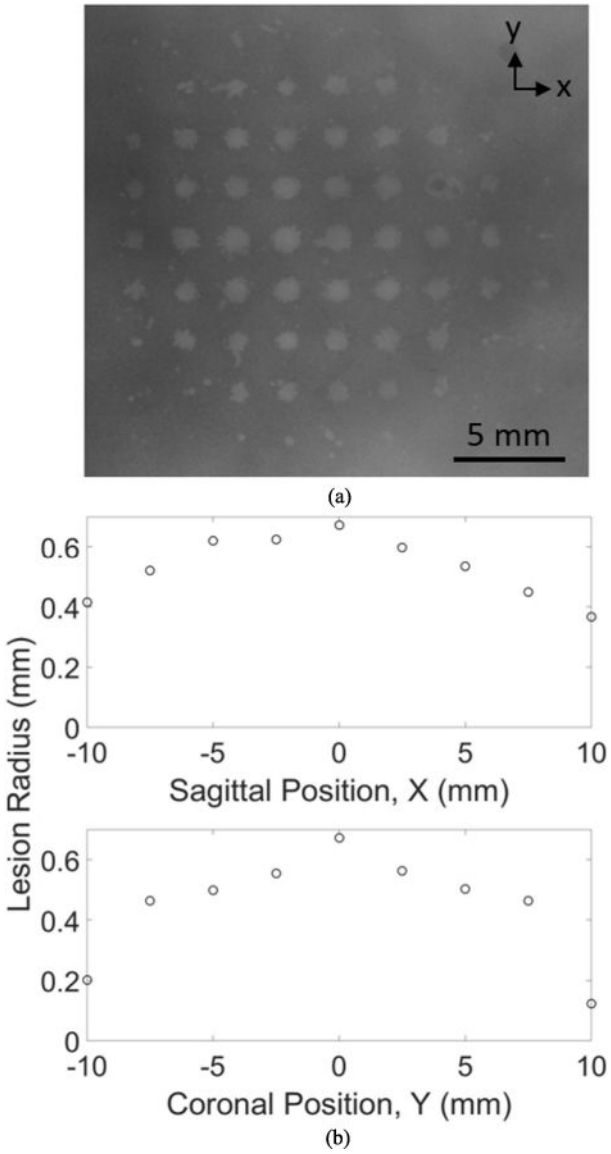

Fig. 10.

(a) Discrete lesions generated in an RBC phantom with electronically steered transcranial histotripsy after single point catheter hydrophone aberration correction. The lesion diameter plotted as a function of position along the (b) sagittal axis coronal axis.

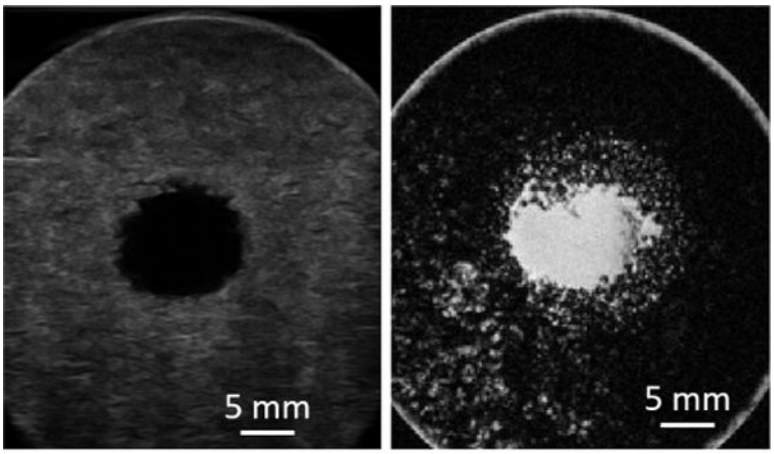

Fig. 11.

Posttreatment (a) ultrasound (b) T2-weighted MR images of the sagittal-coronal plane a clot after electronically steered histotripsy treatment with catheter hydrophone aberration correction.

Fig. 12.
The gross morphology of posttreatment clot after draining liquefied volume.

Table I

−6 dB beam widths obtained by operating the array without catheter hydrophone AC, with AC in the absence of aberration.

	Sagittal	Coronal	Axial
Without AC	4.6 mm	2.2 mm	8 mm
With AC	2.2 mm	2.2 mm	4.4 mm
No Aberration	1.5 mm	1.5 mm	3 mm

Table II

The percentage change in the peak-negative pressure between measurements with without catheter hydrophone aberration correction for each steering direction.

	−20 mm	−10 mm	−5 mm	5 mm	10 mm	20 mm
Sagittal	−8%	36%	50%	61%	43%	−59%
Coronal	61%	27%	37%	61%	52%	0%
Axial	18%	60%	57%	–	–	–

IEEE Trans Ultrason Ferroelectr Freq Control. Author manuscript; available in PMC 2018 November 01.